Scientific Reports

https://doi.org/10.1038/s41598-026-39085-3

Article in Press

Nanoarchitectonics of aptamer-based electrochemical sensor using electrospun carbon nanofibers and Au nanoparticles for cd (II) analysis

Received: 30 August 2025

Accepted: 2 February 2026

Published online: 16 February 2026

Cite this article as: Niknam S., Shabani-Nooshabadi M. & Adabi M. Nanoarchitectonics of aptamer-based electrochemical sensor using electrospun carbon nanofibers and Au nanoparticles for cd (II) analysis. *Sci Rep* (2026). https://doi.org/10.1038/s41598-026-39085-3

Sedigheh Niknam, Mehdi Shabani-Nooshabadi & Mahdi Adabi

Nanoarchitectonics of Aptamer-based Electrochemical Sensor using Electrospun Carbon Nanofibers and Au Nanoparticles for Cd (II) Analysis

Sedigheh Niknam[1], Mehdi Shabani-Nooshabadi[1,2*], Mahdi Adabi[3,4*]

[1] Institute of Nano Science and Nano Technology, University of Kashan, Kashan, Iran

[2] Department of Analytical Chemistry, Faculty of Chemistry, University of Kashan, Kashan, Iran

[3]Department of Medical Nanotechnology, School of Advanced Technologies in Medicine, Tehran University of Medical Sciences, Tehran, Iran

[4]Food Microbiology Research Center, Tehran University of Medical Sciences, Tehran, Iran

Corresponding author email:m.shabani@kashanu.ac.ir, madabi@tums.ac.ir

Abstract

Cadmium(II) is recognized as a hazardous heavy metal with severe implications for both the environment and human health. Traditional detection techniques, including atomic absorption spectroscopy and mass spectrometry, tend to be labor-intensive and require sophisticated instrumentation. In this study, we introduce a new electrochemical biosensor constructed from electrospun carbon nanofibers (CNFs) and gold nanoparticles (AuNPs) for the rapid and sensitive identification of Cd(II). The CNFs were synthesized from polyacrylonitrile (PAN) via a two-step thermal process involving stabilization and carbonization, and their structure was validated through X-ray diffraction and Raman spectroscopy.The synthesized nanofibers were utilized to modify the surface of a screen-printed carbon electrode (SPCE), followed by the electrodeposition of AuNPs to enhance its electrochemical performance. The surface morphology and elemental composition of the modified electrode were characterized using field emission scanning electron microscopy (FESEM) and energy-dispersive X-ray spectroscopy (EDS). A cadmium-selective aptamer was immobilized on the electrode and assessed using cyclic voltammetry (CV). The finalized aptasensor demonstrated a linear detection range from 0.5 to 10 ppb for Cd(II), achieving a detection

limit of 0.05 ppb as measured by differential pulse voltammetry (DPV). The relative standard deviation (RSD) values for repeatability and reproducibility were about 3.2% and 3.5%, respectively.Therefore, this aptasensor can be considered as a promising tool for accurate environmental monitoring of Cd(II).

Keywords: Cadmium, Aptamer, Electrochemical biosensor, Gold nanoparticles, Carbon nanofibers

1. Introduction

Cadmium is a notorious environmental pollutant, prevalent in water, soil, and air, and is known for its high toxicity and tendency to accumulate in living organisms[1-5]. Due to its harmful effects, strict international standards have been established to limit Cd(II) concentrations in food and drinking water[6]. For example, the Joint FAO/WHO Expert Committee on Food Additives has set a monthly intake limit of 25 mg/kg body weight, while the Codex Alimentarius Commission restricts Cd(II) in polished rice to 0.4 mg/kg. The permissible concentration in drinking water is capped at 3.0 µg/L by national and international guidelines[7-10].

Over recent years, multiple analytical approaches have been adopted to detect and control Cd(II) contamination in environmental and biological matrices. These include atomic absorption spectroscopy (AAS)[11],

fluorometry[12,13], inductively coupled plasma emission spectroscopy (ICP-AES)[14], inductively coupled plasma mass spectrometry (ICP-MS)[15], synchrotron radiation X-ray techniques[16]. While these methods are effective, they often demand advanced equipment and skilled personnel, resulting in high costs and lengthy procedures. Consequently, there is a critical need for rapid, cost-effective, and user-friendly alternatives for Cd(II) detection in diverse samples.

DNA's inherent ability to recognize and bind to a diverse array of chemicals and ions has positioned it as a promising tool for the development of sensitive and selective biosensors. Biosensors often employ DNA aptamers, single-stranded DNA molecules with unique secondary structures, to bind target analytes with high affinity selectively. This approach enables the detection of specific molecules or ions within complex samples. Aptamers, designed to recognize and bind target analytes, are crucial components of biosensors. They offer high selectivity and sensitivity, allowing for the detection of even trace amounts of target substances, such as Cd(II), in the presence of interfering species. Electrochemical biosensors, incorporating aptamers as recognition elements, provide a rapid and sensitive analytical technique for detecting Cd(II) at the molecular level. The combination of aptamers and electrochemical detection offers a promising approach to developing reliable and efficient biosensors[1].

The SELEX process has enabled the creation of aptamers, short, single-stranded DNA or RNA molecules, with high specificity for their targets. Recent advancements in SELEX methodology have resulted in aptamer

libraries with enhanced affinity and specificity, thereby facilitating faster selection times and increased success rates. Furthermore, the incorporation of nanomaterials onto electrode surfaces has significantly augmented the sensitivity of biosensors. Nanomaterials such as carbon nanotubes, metal nanoparticles, and graphene provide benefits like increased surface area, improved electron transfer, and better biocompatibility. By modifying electrode surfaces with these nanomaterials, researchers have achieved lower limits of detection (LODs) for various analytes, making these sensors more sensitive and reliable[17,18].

Biosensors utilize a diverse array of nanostructures, including metal nanoparticles, nanotubes, nanocomposites, and nanowires[19].Among these, AuNPs are particularly effective in electrochemical biosensing applications[20]. Advances in nanotechnology have enabled the engineering of materials with tailored properties, facilitating the development of innovative biosensors[21-25]. A can self-assemble on AuNPs, making them ideal for immobilizing bioreceptors. The strong interaction between adenine (A) and AuNPs allows for the formation of dense and organized DNA monolayers. This strategy leverages the programmable nature of single-stranded DNA on noble metal surfaces, enabling the creation of stable and well-defined biorecognition interfaces. The affinity of nucleotides for nanoparticles is ranked as A ≥ G ≈ C > T. When gold is present, adenine (A) binds directly to the Au-surface, while thymine (T) adopts vertically, facilitating direct detection without additional labeling[26,27].

Electrospinning is a versatile method for fabricating micro- and nanofibers. This straightforward technique uses a high-voltage power supply to charge a polymer solution, which is then expelled from a nozzle toward a grounded collector. As the charged jet travels, the solvent evaporates, stretching and solidifying the polymer into fine fibers that are collected on the target surface. Electrospun nanofibers possess desirable features such as high surface-to-volume ratios, robust mechanical strength, and high uniformity[27,28].

Innovative electrochemical sensors for Cd(II) detection exhibit significant advancements in sensitivity and practical performance by integrating nanomaterials and immobilization strategies[29,30]. We developed an electrochemical aptasensor distinguishes itself by combining CNFs with electrodeposited AuNPs to form a nanocomposite electrode that enhances electron transfer and surface area, resulting in a remarkably low detection limit of 0.05 ppb for Cd(II), outperforming many prior sensors. This improvement is further supported by the use of a polyA tail in the aptamer sequence, enabling direct, stable, and high-density immobilization on AuNPs, which overcomes traditional thiol-based aptamer attachment limitations such as desorption and steric hindrance. Compared to other sensors such as those using AuNPson multilayer Nb4C3Tx-modified electrodes (LOD 0.08 μg/L)[31], sulphur-doped carbon nanospheres (LOD ~14.4 μM)[32], reduced graphene oxide/graphitic carbon nitride nanocomposites with aptamers (LOD 0.337 nM)[33], Fe3O4-PEI-Au nanocomposites (LOD 0.01 nM)[34], and dual amplification strategies employing graphene oxide and AuNPs(LOD 0.15 μg/L)[35], this integrated

CNF-AuNPs platform offers an optimal balance of sensitivity, robustness, and practical applicability. While ultra-sensitive detection is valuable, considerations such as fabrication ease, cost, and scalability remain crucial for real-world deployment, positioning this novel sensor as a promising candidate for environmental Cd(II) monitoring with enhanced operational robustness. This study lies in the combination of electrospun CNFs and AuNPs with a polyA-based aptamer immobilization strategy, enabling a sensitive, selective, reproducible, and stable electrochemical sensor for rapid cadmium detection with a very low detection limit and practical sample requirements. It should be noted that combination of CNFs and AuNPs together enhancing sensor sensitivity and stability and enable stable aptamer immobilization via polyadenine binding. Fig. 1 presents a schematic illustration of the SCPE surface modification process alongside the corresponding electrochemical characterization.

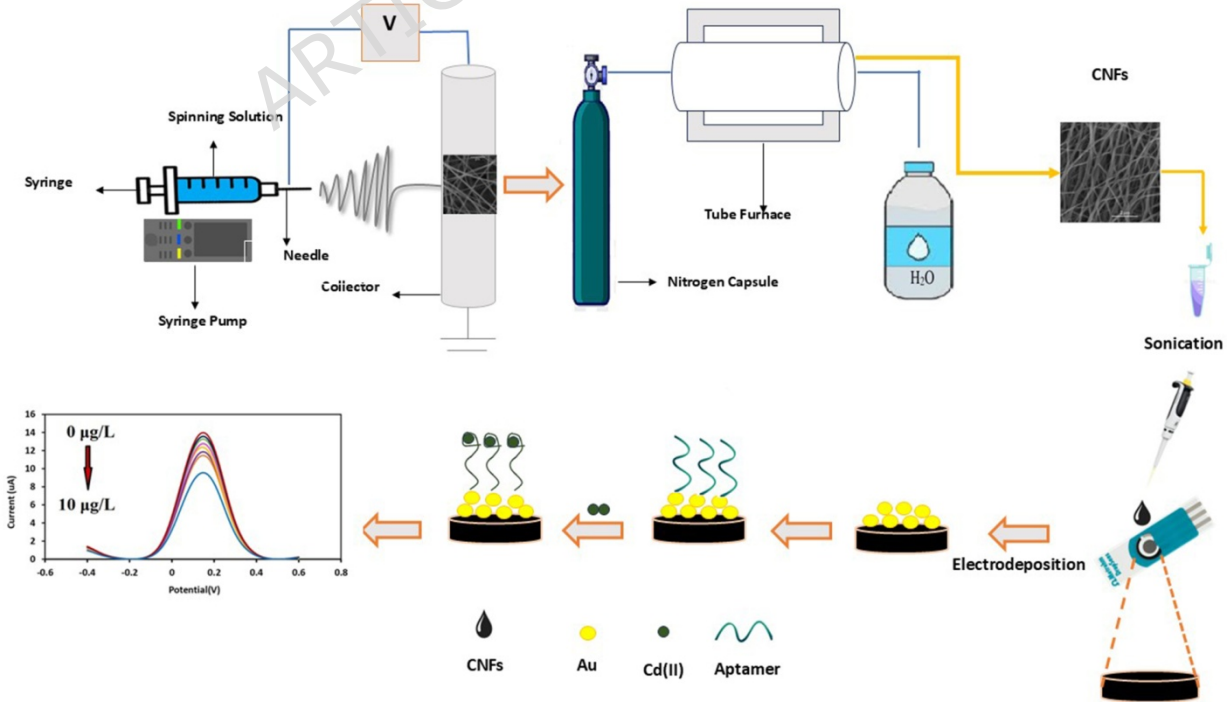

Fig.1. Schematic representation of the SCPE modification and electrochemical analysis

2. Experimental

Materials

All chemicals, including potassium ferrocyanide ($K_4[Fe(CN)_6]$, ≥99.0%), potassium ferricyanide ($K_3[Fe(CN)_6]$, ≥99.0%), potassium dihydrogen phosphate (KH_2PO_4, 99.5%), disodium hydrogen phosphate (Na_2HPO_4, 99.99%), sulfuric acid (H_2SO_4, ≥98.0%), cadmium standard, nitrilotriacetic acid (NTA, 99%), and poly(acrylic acid-co-maleic acid) (PMA, 50 wt.% in H_2O), were sourced from Sigma-Aldrich. The phosphate buffer solutions (PBS) were prepared by 0.1 M Na_2HPO_4 and 0.1 M KH_2PO_4. Chloroauric acid ($HAuCl_4$, 99.99%) and polyacrylonitrile (PAN, MW = 1.5×10^5 g/mol) were obtained from Iranian Polyacrylic Corporation. The aptamer sequence used was 5′-AAAAAAAAAATTTTTGGACTGTTGTGGTATTATTTTTGGTTGTGCAGTATG-3′, featuring a 10-adenine and 5-thymine tail at the 5′ end. All solutions were prepared with ultrapure water.

Instrumentations

Electrochemical analyses were carried out using a μStat 400 Potentiostat/Galvanostat (Dropsens, Spain). Screen-printed carbon electrodes (SPCEs), equipped with Ag/AgCl reference, working, and counter electrodes, were purchased from MetrohmDropSens (Spain). The dimensions of the SPCE are 34 mm in length, 10 mm in width, and 0.5 mm in thickness. Carbon nanofibers (CNFs) were fabricated using an

electrospinning apparatus from Fanavaran Nano Meghyas Ltd., Co. (Iran). The carbonization of fibers was performed in a tube furnace (Iran).

3. Method

Preparation of CNFs

PAN was dissolved in DMF at 40 °C with continuous magnetic stirring (600 rpm) for 12 hours to yield a homogeneous solution, which was then transferred to 10 mL syringes fitted with 18-gauge needles. Electrospinning was conducted by applying high voltage between the needle and a grounded collector, resulting in the formation of nanofibers. The effects of electrospinning parameters such as polymer concentration, needle-to-collector distance, flow rate, applied voltage, and drum speed on fiber morphology and diameter were systematically examined. The optimal condition (solution 8) was identified as 10% (w/v) PAN, 16 kV, 12 cm distance, 1 mL/h flow rate, and 250 rpm, which produced the finest fibers. The collected PAN nanofibers were stabilized at 290 °C in air for 4 hours (heating rate: 1.5 °C/min), then carbonized at 1000 °C for 1 hour under nitrogen (heating rate: 4 °C/min)[36].

Electrode modification of CNFs

A dispersion of CNFs (7 mg/mL in DMF) was sonicated for 2 hours and then stirred magnetically for 1 hour to ensure uniformity. Next, 7 µL of this dispersion was released onto the surface of SPCE and dried for 3 hours (at 60 °C). The electrode was rinsed with 0.1 M PBS to remove any unattached nanofibers. AuNPs were then electrodeposited onto the CNF-coated SPCE by applying a constant potential of -0.4 V for 30 seconds.

Electrode modification of Poly (acrylic acid-co-maleic acid) (PMA) Polymer solution

A 0.05 M PMA solution was prepared in deionized water. A 7 µL aliquot was placed on the SPCE and allowed to dry at room temperature for 3 hours. The electrode was rinsed with 0.1 M PBS to eliminate excess PMA, and AuNPs were electrodeposited at -0.4 V for 30 seconds.

Characterization of the Synthesized Nanofibers and Modified Electrodes

The surface morphology and elemental composition of the screen-printed carbon electrodes (SPCEs) modified with bare CNFs and AuNPs-decorated CNFs were analyzed using field emission scanning electron microscopy (FESEM) coupled with energy-dispersive X-ray spectroscopy (EDX). The average diameter of the nanofibers was determined using SemAforesoftware. Structural characterization of the CNFs was carried out via X-ray diffraction (XRD) using a Philips PW1730 diffractometer (Cu Kα radiation, λ = 1.5406 Å, 40 kV, 30 mA, scanning range 10°–80° 2θ, step size 0.05°). Raman spectroscopy was employed to evaluate the vibrational modes and structural features of the carbon nanofibers.

Aptamer Immobilization on AuNPs/CNFs/SPCE

To immobilize the aptamer, 7 µL of the aptamer solution was dropped onto the modified (Apt/AuNPs/CNFs/SPCE) and incubated overnight at 4 °C. After incubation, the electrode was thoroughly washed with 0.1 M PBS to remove any unbound aptamer.

Electrochemical Characterization (CV and DPV)

The modified electrodes were evaluated by CV and DPV in a solution containing 0.5 M $[Fe(CN)_6]^{3-/4-}$ and 0.1 M PBS (pH 7.4). The potential window was set from -0.4 V to 0.6 V at a scan rate of 50 mV/s. These measurements assessed electron transfer kinetics, surface coverage, and aptamer-target binding affinity.

Cadmium Detection Procedure

The analytical performance of the aptasensor was tested by first exposing it to a 5 µM Cd(II) solution and recording the electrochemical response until a stable current was observed. For calibration, Cd(II) solutions at various concentrations (0.5, 1, 2, 3, 4, 5, and 10 µg/L) were prepared in 0.1 M PBS (pH 7.4). Each solution was incubated with the aptasensor at 4 °C for 30 minutes to allow complex formation between CNFs/AuNPs/Apt and Cd(II). After incubation, the electrode was rinsed with 0.1 M PBS to remove unbound Cd(II), ensuring that the electrochemical signal was due to aptamer conformational changes upon Cd(II) binding.

The limit of detection (LOD) was determined using the equation:

$$LOD = 3\sigma/a$$

where “a” is the slope of the calibration curve and “σ” is the standard deviation of the y-intercept from the linear regression. LOD was calculated from three independent sensors (n = 3)[37].

4. Results and discussion

Nanofibers Characterization

The influence of key electrospinning parameters on nanofiber morphology was investigated.As shown in Table 1 (experiments 1-3) and Fig. S1 (1-3), a decrease in PAN concentration from 14% to 10% resulted in a reduction in nanofiber diameter from approximately 292 nm to 196 nm. This trend can be attributed to a decrease in solution viscosity, leading to increased polymer chain mobility and reduced entanglement, ultimately resulting in the formation of thinner fibers [38,39]. Maintaining a constant 10% concentration, experiments 1, 4-5 (Table 1) and Fig. S1 (4-5) demonstrated that increasing the distance between the needle tip and the collector from 12 to 16 cm led to a decrease in fiber diameter from approximately 196 nm to 144 nm. This phenomenon can be attributed to the formation of multiple jets from the initial droplet, leading to thinner fibers as the distance increases[40].

As depicted in Table 1 (experiments 1, 8-9) and Fig. S1 (8-9), the transition from a decrease in fiber diameter at lower voltages (12-16 kV) to an increase at higher voltages (16-20 kV) illustrates how electrospinning parameters interact. As voltage increases from 12 kV to 16 kV, there is a notable increase in electrostatic forces acting on the polymer jet. This increase results in enhanced electrostatic repulsion among charged particles within the jet, effectively stretching and reducing its diameter. The tensile force exerted on the jet further elongates it, contributing to this reduction in size[41-43]. Additionally, at lower voltages, instability may lead to irregularities such as bead formation; however, at around 16 kV, stability improves enough to produce more uniform fibers while maintaining a decrease in diameter due to increased charge density[41,44]. Conversely,

when the voltage is raised from 16 kV to 20 kV, stronger forces induce a higher rate of fluid ejection from the nozzle. This results in a thicker jet and thus an increase in fiber diameter[41,45]. Although electrostatic forces still act on the jet at these higher voltages, they also contribute to greater initial diameters due to increased fluid dynamics and turbulence within the electrospinning setup. Such turbulence can destabilize the jet further and lead to thicker fibers as additional material is drawn into the electric field[44,46]. Furthermore, the viscoelastic properties of the polymer solution play a critical role; if sufficiently viscous and elastic at higher voltages, these solutions can resist excessive stretching and accumulate more material before being formed into finer fibers[39,41,45].

Finally, an increase in the flow rate, while keeping other parameters constant, increasedthe nanofiber diameter (Fig. S1, Table 1, experiments 1, 6-7). This observation can be attributed to the increased volume of polymer solution ejected from the needle tip at higher flow rates[47]. The greater volume of solution leads to thicker fibers as the jet solidifies.

Table 1: Data from electrospinning of PAN nanofibers

No.	PAN concentration (wt.%)	Distance between tip to collector (cm)	Flow rate (mL/h)	Voltage (kV)	Mean diameter of nanofibers (nm) ± SD	Morphology
1	10	12	1	20	196±68	Nanofiber
2	12	12	1	20	205±46	Nanofiber

3	14	12	1	20	292±85	Nanofiber
4	10	16	1	20	192±21	Nanofiber
5	10	20	1	20	144±44	Nanofiber
6	10	12	0.5	20	202±34	Nanofiber
7	10	12	1.5	20	222±59	Nanofiber
8	10	12	1	16	141±27	Nanofiber
9	10	12	1	12	301±32	Nanofiber

As shown in Fig. 2, the heat treatment process significantly reduced the diameter of the CNFs compared to the initial PAN nanofibers. During the stabilization stage, the polymer undergoes a series of chemical reactions, leading to the formation of a more thermally stable ladder-like structure within the nanofibers, particularly at temperatures exceeding 290 °C. Subsequently, the carbonization step, conducted at elevated temperatures, involves the removal of non-carbon elements such as NH_3, HCN, and H_2O, resulting in the formation of a porous carbon network and a concomitant reduction in fiber diameter[47].

Raman spectroscopy was employed to characterize the structural order of the CNFs. The Raman spectrum of the CNFs (Fig. 3B) exhibited two prominent peaks: a prominent G-band at approximately 1583 cm^{-1}, characteristic of graphitic carbon structures, and a D-band at 1361 cm^{-1}, indicative of disordered carbon structures.X-ray diffraction (XRD) analysis was performed to investigate the structural properties of the nanostructures further. A prominent peak was observed at a 2θ value of

approximately 26.6° in the XRD pattern (Fig. 3A), which is characteristic of the (002) plane of graphitic carbon, consistent with previous literature reports[26].

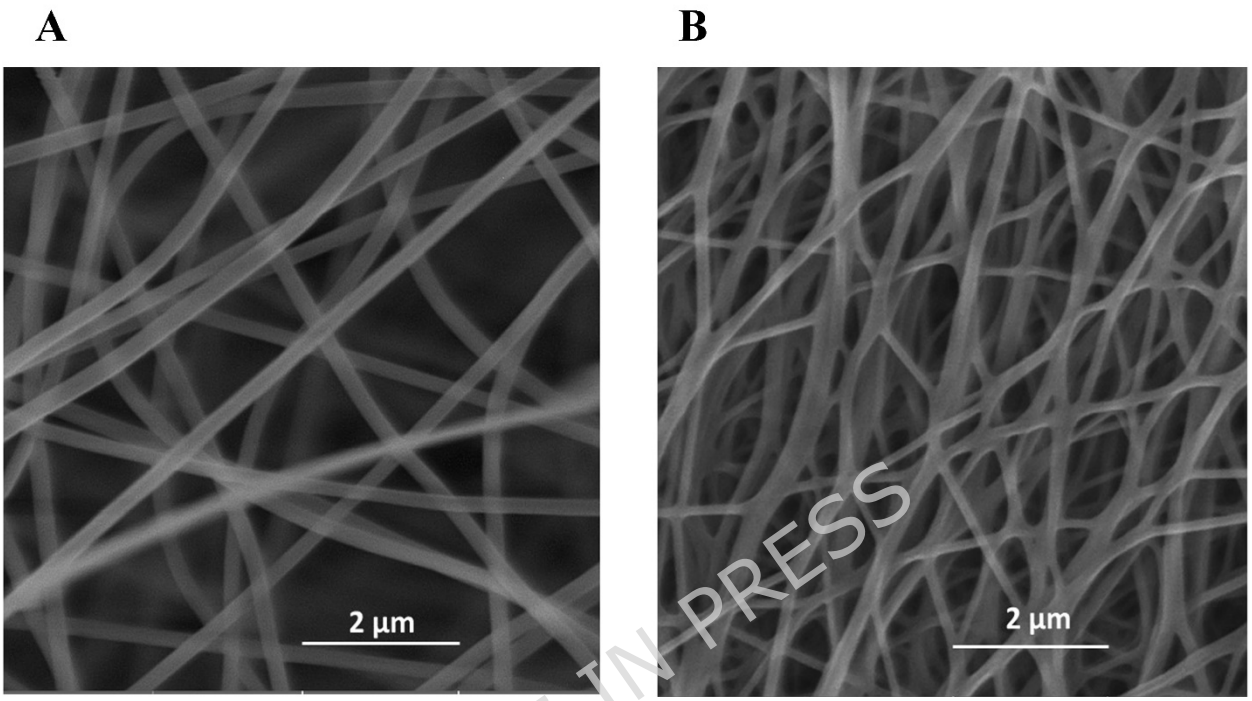

Fig. 2.SEMimages of (A) PAN nanofibers and (B)CNFs.

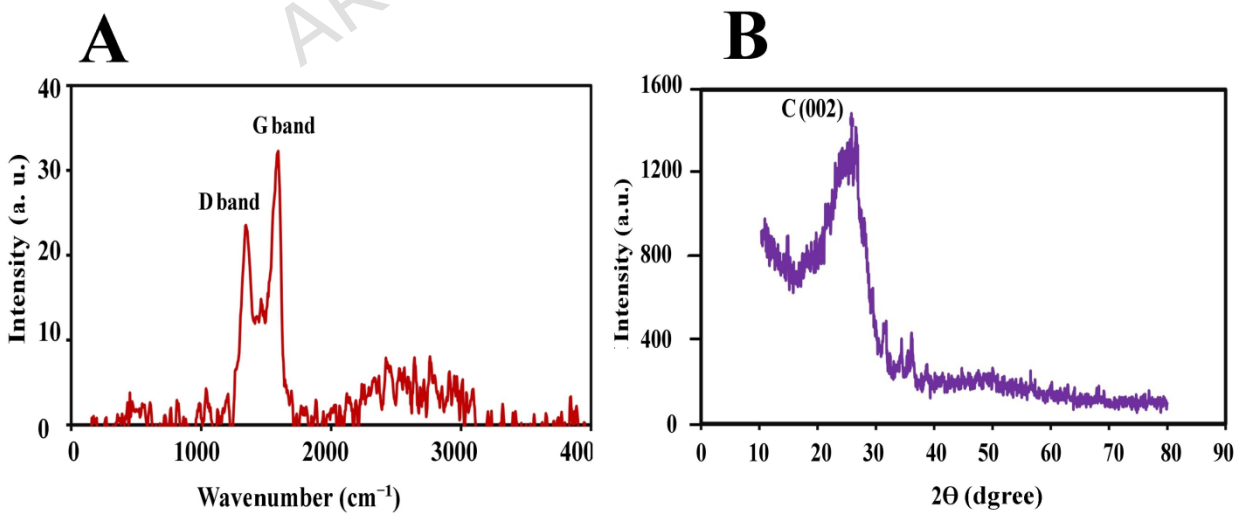

Fig. 3.(A) XRD and (B) Raman spectra of PAN-based CNFs.

Morphology of modified electrode surface

Fig. 4 presents FESEM images illustrating the morphological modifications of the electrode surface. Fig. 4A shows the unmodified SPCE. Fig. 4 B depicts the electrode surfaces modified with CNFs and Fig. 4D exhibits the electrode surfaces modified with CNFs and AuNPs. EDX analysis, as shown in Fig. 4D, confirmed the presence of both carbon and gold elements on the modified electrode surface. The EDX spectrum revealed a higher relative abundance of carbon compared to gold, indicating the successful deposition of AuNPs onto the underlying CNF layers[48].

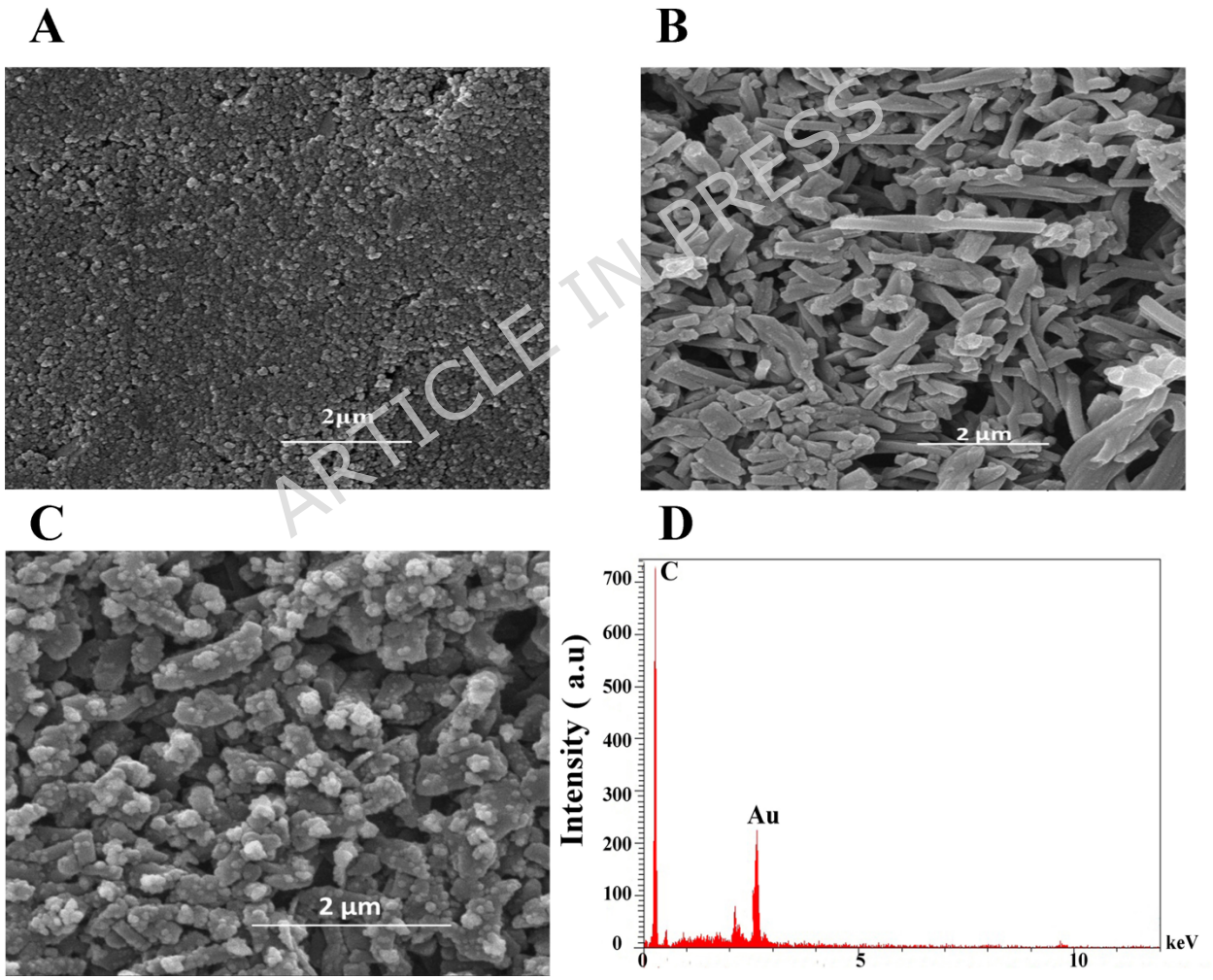

Fig.4.FESEM images of A) bare SPCE, B) CNFs/SPCE, C) AuNPs/CNFs/SPCE, and D) EDX analysis of the AuNPs/CNFs /SPCE.

Electrochemical behavior

The electrochemical properties of the fabricated electrodes were systematically investigated using CV in a solution containing 0.5 M $[Fe(CN)_6]^{3-/4-}$ and 0.1 M phosphate buffer (pH 7.4). The potential window was set from -0.4 V to +0.6 V with a scan rate of 50 mV/s.Starting with the bare screen-printed carbon electrode (SPCE), a pair of well-defined redox peaks was observed, corresponding to the reversible electron transfer of the ferri/ferrocyanide probe. Upon modification with CNFs (Figs. 5A and 5B), the peak current increased from 114.7 µA (SPCE) to 156.5 µA (CNFs/SPCE) significantly, indicating improved electron transfer kinetics and a larger effective surface area due to the nanofiber network[17].As shown in Figs. 5A and 5B, the peak current (156.5 µA)for the 10 wt.% CNF electrode is higher than those for the 12 wt.% (140.9 µA) and 14 wt.% (125.2 µA) electrodes, which can be attributed to the greater surface area of the 10 wt.% CNF. The currentfurther electrodeposition of AuNPs onto the CNF-modified SPCE (Figs. 5C and 5D) resulted in an additional enhancement of the peak current (164.4 µA), demonstrating the additional effect of AuNPs in facilitating charge transfer processes.Following immobilization of the aptamer, which incorporates a poly-A tail (10 bases) and a poly-T spacer sequence (5 bases) at the 5′ end, onto the AuNPs/CNFs/SPCE, a noticeable decrease in peak currents was detected (Figs. 5E and 5F). This decrease is attributed to an increase in charge transfer resistance, a phenomenon commonly observed in aptamer-based biosensors[26]. Optimal aptamer immobilization was achieved with a 5 µM aptamer solution incubated overnight at 4 °C. While the PMA polymer also

demonstrated some conductivity, the electrodeposition of AuNPs onto the PMA-modified surface (Figs. 5G and 5H) was less efficient compared to the CNF-modified surface. Furthermore, the PMA-based aptasensor exhibited significantly poorer analytical performance compared to the CNF-based biosensor.

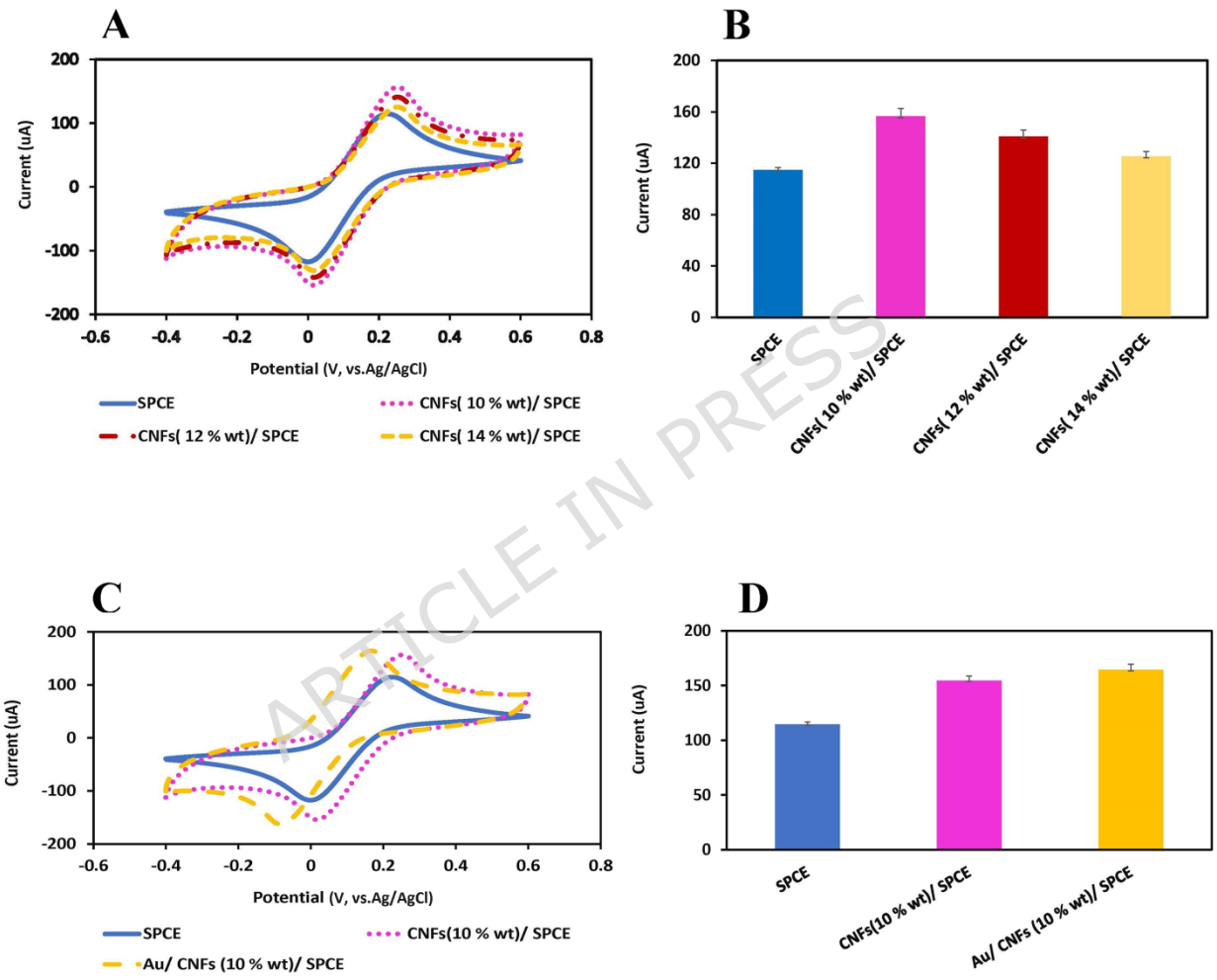

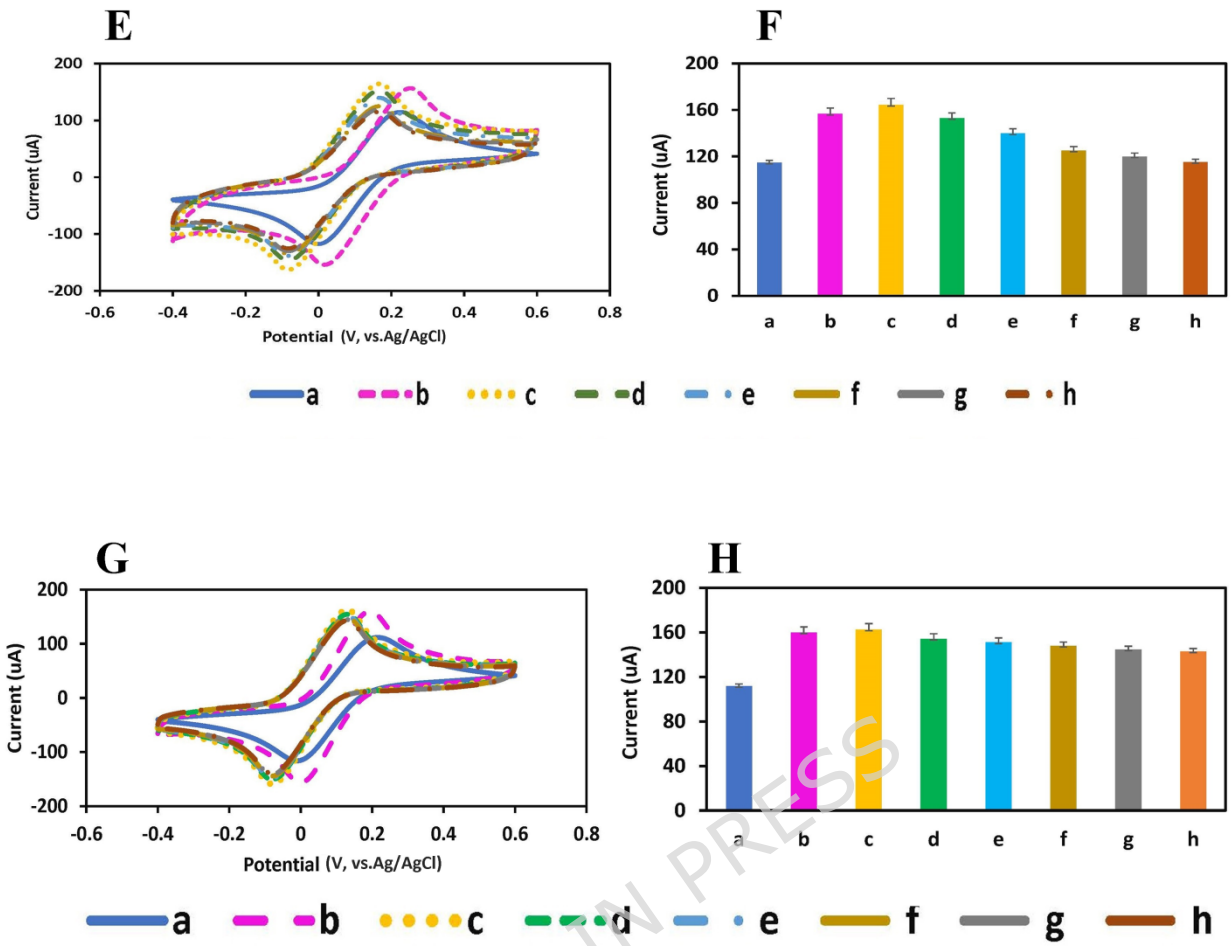

Fig.5. Electrochemical behavior of various modified SPCE. Panel A illustrates the CV responses of CNFs/SPCE electrodes fabricated with different concentrations of PAN solutions. Panel C displays the CV results for AuNPs/CNFs (10 wt.%)/SPCE electrodes. Panel E shows the CV responses for detectingdifferent concentrations of the aptamer with CNFs;a)bare SPCE, b) CNFs (10 wt.%)/SPCE, c) Au/CNFs(10 wt.%)/SPCE, d) Apt(1μM)/Au/CNFs(10 wt.%)/SPCE, e)Apt(2.5 μM)/Au/CNFs(10 wt.%)/SPCE, f) Apt(5 μM)/Au/CNFs(10 wt.%)/SPCE, g) Apt(7.5 μM)/Au/CNFs(10 wt.%)/SPCE, h) Apt(10 μM)/Au/CNFs(10 wt.%)/SPCE. Panel G presents the CV results similar to panel E for different concentrations of aptamers with polymers. The peak currents recorded in

panels B, D, F, and H were after each modification step.All studies used 0.1 M PBS, pH 7.4, in 0.5 M $[Fe(CN)_6]^{3-/4-}$.

Aptasensor performance optimization

Optimizing aptamer concentration is crucial for achieving high sensitivity in Cd(II) detection. As shown in Fig. 5E and 5F, the CV response of the Apt/Au/CNFs/SPCE was evaluated at various aptamer concentrations (1, 2.5, 5, 7.5, and 10 µM).As the concentration increased, the CV responses dropped until 5 µM, the maximum current, was reached. However, further increases beyond the optimal point resulted in a plateau or slight decrease in current, likely due to steric hindrance or non-specific adsorption[49]. Therefore, an aptamer concentration of 5 µM was chosen for subsequent experiments.These results were further confirmed by evaluating different aptamer concentrations directly against the Cd(II) concentration. As shown in Fig. S2, the difference in peak current between Apt(1 µM)/Au/CNFs(10 wt.%)/SPCE and Cd(10 µM)/Apt(1 µM)/Au/CNFs(10 wt.%)/SPCE was 1.68 µA, whereas the difference between Apt(5 µM)/Au/CNFs(10 wt.%)/SPCE and Cd(10 µM)/Apt(5 µM)/Au/CNFs(10 wt.%)/SPCE was 4.42 µA. Increasing the aptamer concentration from 5 to 10 µM did not result in significant differences compared to the range between 5 and 10 µM. Additionally, the current signal remains consistent for Apt/Au/Polymer/SPCE (Fig. 5G, H).

Cadmium detection and calibration chart

Cadmium levels were quantitatively measured by recording the DPV responses of the custom-engineered electrochemical aptasensor under optimized conditions. Cadmium standard solutions were prepared in dilutions ranging from 0.5, 1, 2, 3, 4, 5, and 10 µg/L. Fig. 6 illustrates the

calibration curve for cadmium concentration. The electrode modified with Apt/AuNPs/CNFs/SPCE demonstrated superior performance, exhibiting the highest peak current response. As cadmium concentration increased, the oxidation current decreased. At 10 µg/L, the current peak is the lowest. Upon introducing cadmium at a concentration of 10 µg/L to the electrode (refer to Fig. 6A), the observed peak current drops to its minimum value relative to the aptamer/AuNPs/CNFs/SPCE. This reduction in current is primarily due to the selective interaction between cadmium ions and the aptamer, which triggers structural changes in the aptamer that obstruct electron transfer on the electrode surface[49].

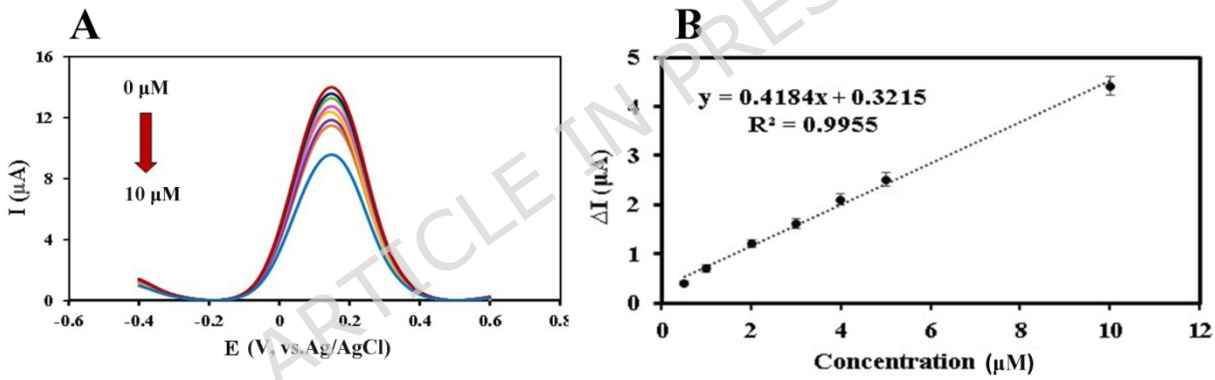

Fig. 6.(A) DPV signals of the aptasensor recorded at Cd(II) concentrations of 0.5, 1, 2, 3, 4, 5, and 10 µg/L. (B) Corresponding linear calibration curve obtained in PBS (0.1 M, pH 7.4), containing 0.5 M $[Fe(CN)_6]^{3-/4-}$.

Figure 6B displays the calibration plot, which illustrates the association of the recorded current (µA) and cadmium concentration (µM). The data reveal a pronounced linear correlation, described by the regression equation I (µA) = 0.4184 C (µM) + 0.3215, with an excellent correlation coefficient (R^2) of

0.9955. The detection limit (LOD) was determined to be 0.05 µg/L, calculated using the equation $3\sigma/a$, that σ refers to the standard deviation of the blank measurements and a represents the slope of the calibration line shown in Fig.6B. Additionally, Table 2 summarizes how the performance of this aptasensor compares to other cadmium detection sensors previously reported in the literature. The incorporation of nanomaterials such as CNFs and AuNPs enhanced electron transfer and stability, resulting in improved detection limits. These attributes underscore the potential of aptasensor for Cd(II) detection.

Table 2: Overview of different electrochemical biosensors and sensing platforms reported for Cd(II) detection.

Detection system	**Technique**	**Linear range (ppb)**	**LOD (ppb)**	**Reference**
GDY/GCE	SWAS	10-1000	0.46	[50]
MB/Apt/Gold Electrode	ACV	250-1000	92	[37]
Apt/AuNPs/CB/SPCE	SWV	1-50	0.14	[49]
ssDNA/Au	CV	1-20	0.3	[17]
PB-PEDOT/LSG/GCE	DPV	1-10000	0.85	[51]
TiO_2/ZrO_2 composite/CPE	SWASV	1-200	0.77	[52]
UiO-66-NH_2@PANI/GCE	CV/DPV	0.5-600	0.3	[53]

Apt/AuNPs/CNFs/SPCE	DPV	0.5-10	0.05	This work

Selectivity, reproducibility,repeatability,and stability:

The aptasensor's repeatability (an aptasensor tested for the same analyte several times under the same conditions) and reproducibility(several aptasensors tested for the same analyte) were determined by measuring its current response to 10 µM cadmium across four consecutive trials using the same electrode. The relative standard deviation (RSD) values for repeatability and reproducibility were found to be approximately 3.2% and 3.5%, respectively, indicating consistent electrode fabrication and performance (Fig. 7A for reproducibility). Long-term stability was assessed by monitoring the aptamer-modified electrode after storage at 4 °C for 30 days. The sensor retained 97% ± 1% (n = 3) of its initial current response, highlighting the excellent durability and stability of the developed aptasensor(Fig. 7B)[22]. Ensuring the selectivity of the cadmium-specific aptamer is essential for the aptasensor's precision and dependability. To evaluate this, the sensor's differential pulse voltammetry (DPV) responses were recorded in the presence of eight potentially interfering metal ionsnamely Ca(II), Mg(II), Zn(II), Pb(II), Fe(III), Ag(I), Cu(II), and Mn(II)—each at a concentration of 5 µM (Fig. 7C and D). The reason for this ions is that Ca(II) and Mg(II) are abundant in natural waters and biological systems, often complicating trace cadmium detection due to their high concentrations[54]. Zn(II) and Pb(II) commonly coexist with cadmium in industrial and environmental samples because of similar pollution

sources[55,56]. Fe(III) and Cu(II) may compete with cadmium for ligand binding sites, affecting detection selectivity[57,58], while Ag(I) and Mn(II) can cause non-specific interactions due to similar ionic radii and charges[59,60]. These interferences can lead to false positives or negatives such as Hg(II)-induced false positives in immunoassays[61].

To further reduce interference, particularly from Hg(II), Pb(II), Cu(II), and Zn(II), 25 μM nitrilotriacetic acid (NTA) was introduced into the solution. The observed interactions can be attributed to the phosphate groups on the aptamer, which have an affinity for certain metal ions like Cu(II) and Zn(II). Nevertheless, the aptasensor was able to selectively identify Cd(II) even in the presence of these eight metals, with NTA effectively minimizing cross-reactivity[49].

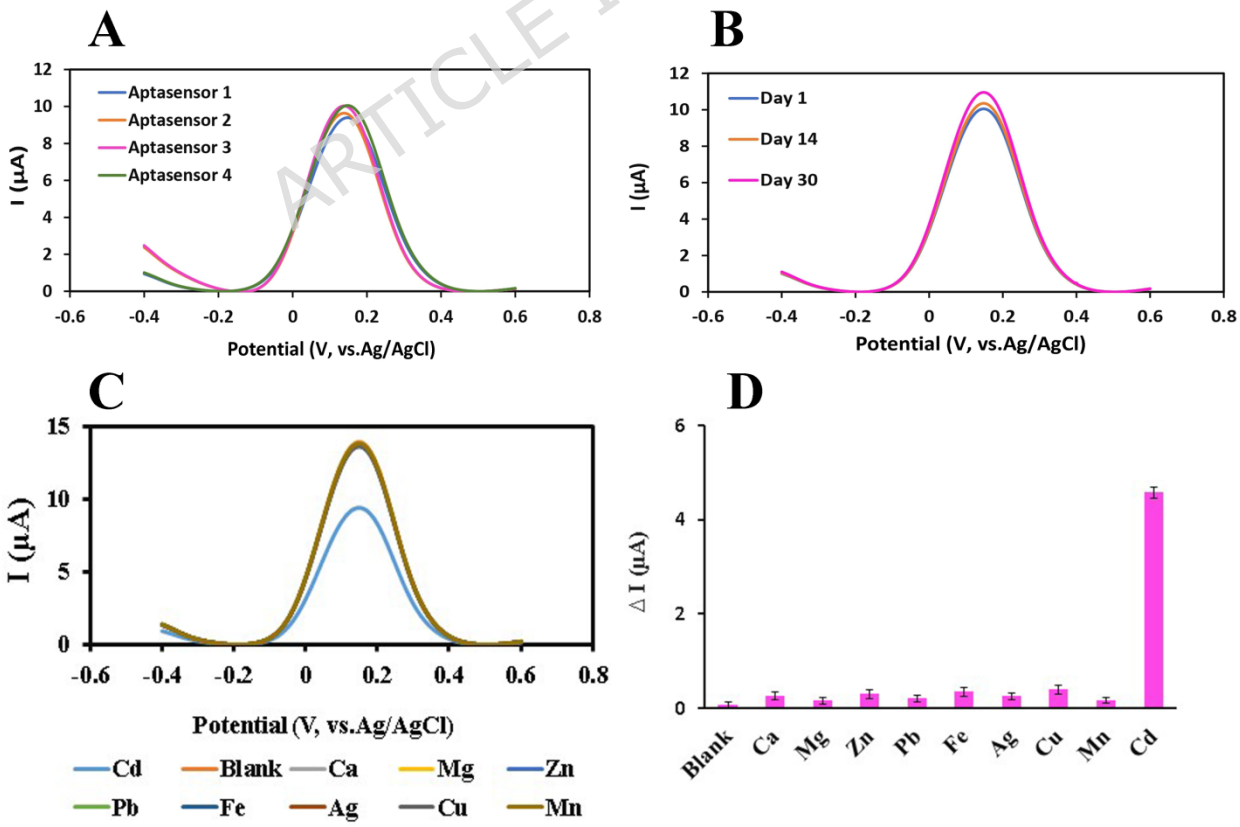

Fig.7.(A) Assessment of the aptasensor's reproducibility for detecting 10 µg/L Cd(II). (B) Evaluation of the sensor's stability for Cd(II) detection over time. (C) Variation in peak current responses of the aptasensor when exposed to 10 µM concentrations of different metal ions and 10 µM Cd(II) in the presence of NTA. All measurements were carried out in 0.1 M phosphate buffer solution (PBS) at pH 7.4, containing 0.5 M $[Fe(CN)_6]^{3-/4-}$ as the redox probe.

Analysis of Real Sample

The performance and accuracy of the proposed method were assessed using the aptasensor for Cd(II) detection in tap water samples diluted with PBS buffer. The obtained results revealed a close agreement between the added and detected Cd(II) concentrations. Recovery rates ranging from 95% to 105% confirmed that the aptasensor performs reliably in complex aqueous matrices and is suitable for the rapid and early detection of Cd(II) in tap water (Table 3).

Table 3. Spike and recovery from tab water diluted PBS

Sample	Added (ppb)	Found (ppb)	Recovery (%)	RSD (%) (n=3)
Tab Water	1.0	0.98	98	2.01
	5.0	0.96	96	2.3
	10.0	10.5	105	2.4
	20	0.95	95	2.9

5. Conclusion

In this research, an innovative electrochemical sensing system for cadmium was created by combining AuNPs with CNFs. The resulting composite material greatly enhanced the electrode's active surface area, allowing for

the attachment of a much larger number of aptamer molecules than is possible with conventional electrode designs.

Instead of relying on thiol-based immobilization, we employed a novel strategy utilizing the inherent binding affinity between poly(A) sequences within the aptamer and the gold nanoparticles. This approach, facilitated by a poly(T) spacer at the 3' end of the aptamer, ensured proper aptamer orientation and minimized steric hindrance.

The resulting biosensor demonstrated several key advantages, including rapid response times, high sensitivity, excellent selectivity, and good stability and reproducibility. Furthermore, the biosensor requires only a small sample volume (5 µL), making it a practical and cost-effective solution for cadmium detection. These findings highlight the potential of this novel approach for the development of sensitive and reliable point-of-care diagnostic tools.

Acknowledgements

This work was supported by University of Kashan, Iran.During the preparation of this work, the authors used AI (perplexity.ai) in the writing process to improve the readability and language of the manuscript. After using this AI, the authors reviewed and edited the content as needed and take full responsibility for the content of the published article.

Author contributions

S.N.: Investigation, Methodology, Visualization, Writing-original draft. M.S.: Validation, Writing-review & editing, Conceptualization, Supervision. M.A: Supervision, Project administration, Writing-review & editing.

Funding

The authors received no funding for this work.

Competing interests

The authors declare no competing interests.

Data Availability

The datasets used and/or analysed during the current study available from the corresponding author on reasonable request.

References

1 Hayat, M. T., Nauman, M., Nazir, N., Ali, S. & Bangash, N. in *Cadmium toxicity and tolerance in plants* 163-183 (Elsevier, 2019).

2 Bui, M.-P. N., Li, C. A., Han, K. N., Pham, X.-H. & Seong, G. H. Electrochemical determination of cadmium and lead on pristine single-walled carbon nanotube electrodes. *Analytical Sciences* **28**, 699-704 (2012).

3 Koudelkova, Z. *et al.* Determination of zinc, cadmium, lead, copper and silver using a carbon paste electrode and a screen printed electrode modified with chromium (III) oxide. *Sensors* **17**, 1832 (2017).

4 Dai, H., Wang, N., Wang, D., Ma, H. & Lin, M. An electrochemical sensor based on phytic acid functionalized polypyrrole/graphene oxide nanocomposites for simultaneous determination of Cd (II) and Pb (II). *Chemical Engineering Journal* **299**, 150-155 (2016).

5 Sacara, A.-M., Pitzalis, F., Salis, A., Turdean, G. L. & Muresan, L. M. Glassy carbon electrodes modified with ordered mesoporous silica for the electrochemical detection of cadmium ions. *ACS omega* **4**, 1410-1415 (2019).

6 Hui, Y. *et al.* Recent advancements in electrochemical biosensors for monitoring the water quality. *Biosensors* **12**, 551 (2022).

7 Gao, Z. *et al.* Recent aptamer-based biosensors for Cd2+ detection. *Biosensors* **13**, 612 (2023).

8 Cerutti, S., Silva, M., Gasquez, J., Olsina, R. & Martinez, L. On-line preconcentration/determination of cadmium in drinking water on activated carbon using 8-hydroxyquinoline in a flow injection system coupled to an inductively coupled plasma optical emission spectrometer. *Spectrochimica Acta Part B: Atomic Spectroscopy* **58**, 43-50 (2003).

9 Ramalingam, M., Ponnusamy, V. K. & Sangilimuthu, S. N. A nanocomposite consisting of porous graphitic carbon nitride nanosheets and oxidized multiwalled carbon nanotubes for simultaneous stripping voltammetric determination of cadmium (II), mercury (II), lead (II) and zinc (II). *Microchimica Acta* **186**, 69 (2019).

10 Manikandan, R. *et al.* Recent advances in miniaturized electrochemical analyzers for hazardous heavy metal sensing in environmental samples. *Coordination Chemistry Reviews* **499**, 215487 (2024).

11 Golbedaghi, R. *et al.* Determination of cadmium (II) ion by atomic absorption spectrometry after cloud point extraction. *Journal of the Iranian Chemical Society* **9**, 251-256 (2012).

12 Charles, S., Dubois, F., Yunus, S. & Donckt, E. V. Determination by fluorescence spectroscopy of cadmium at the subnanomolar level: application to seawater. *Journal of Fluorescence* **10**, 99-99 (2000).

13 Noh, Y., Jo, E.-J., Mun, H., Ahn, Y.-d. & Kim, M.-G. Homogeneous and selective detection of cadmium ions by forming fluorescent cadmium-protein nanoclusters. *Chemosphere* **174**, 524-530 (2017).

14 Zougagh, M., de Torres, A. G. a. & Pavon, J. C. Determination of cadmium in water by ICP-AES with on-line adsorption preconcentration using DPTH-gel and TS-gel microcolumns. *Talanta* **56**, 753-761 (2002).

15 Karunasagar, D. & Arunachalam, J. Determination of cadmium by inductively coupled plasma mass spectrometry-reduction of molybdenum oxide interferences by addition of acetonitrile. *Analytica chimica acta* **441**, 291-296 (2001).

16 Monico, L. *et al.* Probing the chemistry of CdS paints in The Scream by in situ noninvasive spectroscopies and synchrotron radiation x-ray techniques. *Science advances* **6**, eaay3514 (2020).

17 Iftikhar, F. J., Shah, A., Wali, Q. & Kokab, T. Advancements in nanofiber-based electrochemical biosensors for diagnostic applications. *Biosensors* **13**, 416 (2023).

18 Zhan, S., Wu, Y., Wang, L., Zhan, X. & Zhou, P. A mini-review on functional nucleic acids-based heavy metal ion detection. *Biosensors and Bioelectronics* **86**, 353-368 (2016).

19 Zhu, D. *et al.* Hydrophobic collapse-driven nanoparticle coating with poly-adenine adhesives. *Chemical Communications* **57**, 3801-3804 (2021).

20 Negahdary, M. Electrochemical aptasensors based on the gold nanostructures. *Talanta* **216**, 120999 (2020).

21 Niknam, S., Dehdast, S. A., Pourdakan, O., Shabani, M. & Koohi, M. K. Tungsten disulfide nanomaterials (WS2 NM) application in biosensors and nanomedicine: a review. *Nanomedicine Research Journal* **7**, 214-226 (2022).

22 Liu, Y. *et al.* Cd-aptamer electrochemical biosensor based on AuNPs/CS modified glass carbon electrode. *Journal of Biomedical Nanotechnology* **13**, 1253-1259 (2017).

23 Manikandan, R. *et al.* Nano-engineered paper-based electrochemical biosensors: Versatile diagnostic tools for biomarker detection. *Coordination Chemistry Reviews* **523**, 216261 (2025).

24 Manikandan, R., Yoon, J.-H. & Chang, S.-C. Emerging Trends in nanostructured materials-coated screen printed electrodes for the electrochemical detection of hazardous heavy metals in environmental matrices. *Chemosphere* **344**, 140231 (2023).

25 Manikandan, R., Mani, S. P., Selvan, K. S., Yoon, J.-H. & Chang, S.-C. Fabrication of S and O-incorporated graphitic carbon nitride linked poly (1, 3, 4-thiadiazole-2, 5-dithiol) film for selective sensing of Hg2+ ions in water, fish, and crab samples. *Food Chemistry* **425**, 136483 (2023).

26 Geravand, M. *et al.* Nanoarchitectonics of aptamer-based electrochemical biosensor utilizing electerospun carbon nanofibers and gold nanoparticles for Acinetobacter baumannii detection. *Microchemical Journal* **200**, 110437 (2024).

27 Mohammadi, S., Pooshang Bagheri, K., Mousavi Nadushan, R. & Adabi, M. Nanoarchitectonics of electrochemical aptasensor based on electrospun carbon nanofibers and gold nanoparticles for tetracycline detection in chicken ham. *Applied Physics A* **129**, 176 (2023).

28 Esnaashari, S. S. *et al.* Preparation and characterization of kefiran electrospun nanofibers. *International journal of biological macromolecules* **70**, 50-56 (2014).

29 Li, W. *et al.* A self-template strategy for the synthesis of mesoporous carbon nanofibers as advanced supercapacitor electrodes. *Adv. Energy Mater* **1**, 382-386 (2011).

30 Zhao, Q. *et al.* One dimensional silver-based nanomaterials: preparations and electrochemical applications. *Small* **13**, 1701091 (2017).

31 Zhang, Z., Karimi-Maleh, H. & Jahanabadi, N. Z. in *International Conference on Optoelectronic Materials and Devices (ICOMD 2023).* 18-24 (SPIE).

32 Varshney, R., Pavithra, N., Singh, S., Naik, T. S. K. & Ramamurthy, P. C. in *2022 IEEE International Conference on Emerging Electronics (ICEE).* 1-4 (IEEE).

33 Wang, X. *et al.* A novel aptasensor based on graphene/graphite carbon nitride nanocomposites for cadmium detection with high selectivity and sensitivity. *ACS Applied Nano Materials* **1**, 2341-2346 (2018).

34 Lai, Z., Mahdavi, B. & Baghayeri, M. Label-free and sensitive determination of toxic Cd (II) in environmental waters using a Fe3O4-PEI-Au based electrochemical aptasensor. *Alexandria Engineering Journal* **83**, 251-256 (2023).

35 Yin, F. *et al.* Ultrasensitive Imprinted Limited Domain Electrochemical Biosensor Based on a Dual Signal Amplification Strategy of Gocs Composites and Gold Nanoparticles for Selective Cd2+ Detection. *Available at SSRN 4611900*.

36 Faridi-Majidi, R., Ziyadi, H., Naderi, N. & Amani, A. Use of artificial neural networks to determine parameters controlling the nanofibers diameter in electrospinning of nylon-6, 6. *Journal of applied polymer science* **124**, 1589-1597 (2012).

37 Zhad, H. R. L. Z., Torres, Y. M. R. & Lai, R. Y. A reagentless and reusable electrochemical aptamer-based sensor for rapid detection of Cd (II). *Journal of Electroanalytical Chemistry* **803**, 89-94 (2017).

38 Jia, Y.-T. *et al.* Fabrication and characterization of poly (vinyl alcohol)/chitosan blend nanofibers produced by electrospinning method. *Carbohydrate polymers* **67**, 403-409 (2007).

39 Thompson, C., Chase, G. G., Yarin, A. & Reneker, D. Effects of parameters on nanofiber diameter determined from electrospinning model. *Polymer* **48**, 6913-6922 (2007).

40 Adabi, M., Saber, R., Faridi-Majidi, R. & Faridbod, F. Performance of electrodes synthesized with polyacrylonitrile-based carbon nanofibers for application in electrochemical sensors and biosensors. *Materials science and engineering: C* **48**, 673-678 (2015).

41 Kalluri, L., Satpathy, M. & Duan, Y. Effect of electrospinning parameters on the fiber diameter and morphology of PLGA nanofibers. *Dental Oral Biology and Craniofacial Research* **4** (2021).

42 Ma, M. *et al.* Analysis and prediction of electrospun nanofiber diameter based on artificial neural network. *Polymers* **15**, 2813 (2023).

43 Beachley, V. & Wen, X. Effect of electrospinning parameters on the nanofiber diameter and length. *Materials Science and Engineering: C* **29**, 663-668 (2009).

44 Bakar, S., Fong, K., Eleyas, A. & Nazeri, M. in *IOP Conference Series: Materials Science and Engineering*. 012076 (IOP Publishing).

45 El-Hadi, A. M. & Al-Jabri, F. Y. Influence of electrospinning parameters on fiber diameter and mechanical properties of poly (3-hydroxybutyrate)(PHB) and polyanilines (PANI) blends. *Polymers* **8**, 97 (2016).

46 In-Bo, S. & Taejoon, K. Effects of electrospinning nozzle size and voltage on polyvinylpyrrolidone fiber structure formation. (2020).

47 Salimi, M. *et al.* Electrochemical immunosensor based on carbon nanofibers and gold nanoparticles for detecting anti-Toxoplasma gondii IgG antibodies. *Microchimica Acta* **190**, 367 (2023).

48 Mohamed, H. M. Screen-printed disposable electrodes: Pharmaceutical applications and recent developments. *TrAC Trends in Analytical Chemistry* **82**, 1-11 (2016).

49 Fakude, C. T., Arotiba, O. A. & Mabuba, N. Electrochemical aptasensing of cadmium (II) on a carbon black-gold nano-platform. *Journal of Electroanalytical Chemistry* **858**, 113796 (2020).

50 Li, Y. *et al.* Electrochemical sensor based on graphdiyne is effectively used to determine Cd2+ and Pb2+ in water. *Sensors and Actuators B: Chemical* **332**, 129519 (2021).

51 Machhindra, L. A. & Yen, Y.-K. A Highly sensitive electrochemical sensor for Cd2+ detection based on prussian blue-PEDOT-loaded laser-scribed graphene-modified glassy carbon electrode. *Chemosensors* **10**, 209 (2022).

52 Nguyen, P. K. Q. & Lunsford, S. K. Square wave anodic stripping voltammetric analysis of lead and cadmium utilizing titanium dioxide/zirconium dioxide carbon paste composite electrode. *Journal of Electroanalytical Chemistry* **711**, 45-52 (2013).

53 Wang, Y. *et al.* A metal–organic framework and conducting polymer based electrochemical sensor for high performance cadmium ion detection. *Journal of Materials Chemistry A* **5**, 8385-8393 (2017).

54 Sasaki, Y., Yamamoto, N., Suzuki, Y., Ueta, I. & Kawakubo, S. Kinetic spectrophotometric determination of trace cadmium in environmental

fresh water with 5, 10, 15, 20-tetraphenyl-21H, 23H-porphinetetrasulfonic acid. *Analytical Sciences* **31**, 551-555 (2015).

55 JS, A. N., S, S. & KY, S. Trace-level detection of Pb (II) and Cd (II) aided by MoS2 nanoflowers and graphene nanosheet combination. *ACS Applied Engineering Materials* **1**, 924-935 (2023).

56 Beas-Bernuy, L. C. *et al.* Cd2+ Detection by an electrochemical electrode based on MWCNT–orange peel activated carbon. *ACS omega* **8**, 37341-37352 (2023).

57 Dong, Y., Ding, L., Jin, X. & Zhu, N. Silver nanoparticles capped with chalcon carboxylic acid as a probe for colorimetric determination of cadmium (II). *Microchimica Acta* **184**, 3357-3362 (2017).

58 Liu, M., Feng, Y., Wang, G. & Fang, B. Determination of cadmium (II) using glassy carbon electrodes modified with cupferron, ß-naphthol, and multiwalled carbon nanotubes. *Microchimica Acta* **177**, 221-228 (2012).

59 Sadia, M. *et al.* Rapid detection of Cd2+ ions in the aqueous medium using a highly sensitive and selective turn-on fluorescent chemosensor. *Molecules* **28**, 3635 (2023).

60 Tang, Y., Liu, H., Jiang, G. & Gu, Z. Highly selective recognition of Cd2+ by an indole derivative chemosensor. *Journal of Applied Spectroscopy* **84**, 911-914 (2017).

61 Khosraviani, M., Pavlov, A. R., Flowers, G. C. & Blake, D. A. Detection of heavy metals by immunoassay: optimization and validation of a rapid, portable assay for ionic cadmium. *Environmental Science & Technology* **32**, 137-142 (1998).